JGR Oceans

RESEARCH ARTICLE
10.1029/2020JC016509

Key Points:

- Sea surface temperatures (SSTs) measure upper ocean temperatures after variability tied to the atmosphere is removed
- Once adjusted for air temperature, SSTs near the fjord reflect deep Atlantic Water (AW) temperatures entering Sermilik Fjord
- Dilution of AW as it intrudes onto the continental shelf modulates nearshore temperatures

Supporting Information:

Supporting Information may be found in the online version of this article.

Correspondence to:

T. Snow,
tasha.snow@colorado.edu

Citation:

Snow, T., Straneo, F., Holte, J., Grigsby, S., Abdalati, W., & Scambos, T. (2021). More than skin deep: Sea surface temperature as a means of inferring Atlantic Water variability on the southeast Greenland continental shelf near Helheim Glacier. *Journal of Geophysical Research: Oceans*, *126*, e2020JC016509. https://doi.org/10.1029/2020JC016509

Received 15 JUN 2020
Accepted 1 APR 2021

More than Skin Deep: Sea Surface Temperature as a Means of Inferring Atlantic Water Variability on the Southeast Greenland Continental Shelf Near Helheim Glacier

T. Snow[1,2], F. Straneo[3], J. Holte[3], S. Grigsby[1,4], W. Abdalati[1,2], and T. Scambos[1]

[1]Cooperative Institute for Research in Environmental Sciences, University of Colorado, Boulder, CO, USA, [2]Geography Department, University of Colorado Boulder, Boulder, CO, USA, [3]Scripps Institution of Oceanography, University of California San Diego, La Jolla, CA, USA, [4]Department of Geophysics, Colorado School of Mines, Golden, CO, USA

Abstract Enhanced outlet glacier discharge accounts for almost half of the Greenland Ice Sheet's mass loss since 1990. Warming subsurface Atlantic Water (AW) has been implicated in much of that loss, particularly along Greenland's southeastern coast. However, oceanographic observations are sparse prior to the last decade, making it difficult to diagnose changes in AW properties reaching the glaciers. Here, we investigate the use of sea surface temperature (SST) measurements to quantify ocean temperature variability on the continental shelf near Sermilik Fjord and Helheim Glacier. We find that after removing the short-term, atmospheric-driven variability in non-winter months, regional SSTs provide a reliable upper ocean (surface mixed layer) temperature record. In the trough region near Sermilik Fjord, the adjusted SSTs correlate well with moored ocean measurements of the water entering the fjord at depth and driving glacier melting. Using this relationship, we reconstruct the AW variability on the shelf dating back to 2000, 8 years before the first mooring deployments. Across the 19-year record, the AW temperatures in the trough do not always track properties in the source waters of the Irminger Current, which flows along the continental break. Instead, the properties of the waters found at the fjord mouth depend on variations in the source AW and, also, in the Polar Water that flows into the region from the Arctic Ocean. Satellite-derived SSTs, when combined with local oceanography considerations, have the potential to improve understanding around previously unanswered glacier-ocean questions in areas surrounding Greenland.

Plain Language Summary Greenland ice contributes one-quarter of global sea level rise each year and almost half of that loss comes from glaciers at its periphery. Warming ocean waters may cause much of that loss. Records produced from ocean instruments are the main method for studying the oceans around Greenland, but few observations exist prior to the last decade. In this work, we investigate the use of sea surface temperatures (SSTs) acquired by satellites to assess ocean temperature changes through time. We explore their use near the southeastern Greenland coast, where warm water circulates from the North Atlantic Ocean onto the continental shelf and eventually reaches Helheim Glacier, Greenland's fifth largest glacier. Through a comparison with ocean instruments, we find that SSTs serve as a good indicator of upper ocean temperatures in this region once proper corrections are applied. With these records, we find that the dilution of warm waters as they circulate from the North Atlantic changes over time and governs the temperature of the water that eventually reaches Helheim, which was previously unknown. Our work shows that SSTs can provide new insight into the ocean changes that may have affected glacier retreat before ocean instruments were deployed.

1. Introduction

The Greenland Ice Sheet and its surrounding oceans have changed rapidly as a result of shifting climate conditions in recent decades (IMBIE Team, 2019). Since the late 1990s, many of Greenland's tidewater glaciers have experienced periods of substantial thinning and retreat, interspersed with periods of greater stability or re-advance (Howat et al., 2008; Moon et al., 2012). Their mass loss derives from a combination of surface mass balance (the net difference between snow accumulation, meltwater runoff, and sublimation; Fettweis et al., 2017; van den Broeke et al., 2009) and dynamical changes that are associated with glacier

acceleration, thinning, and enhanced ice export, or discharge (Enderlin et al., 2014; Mouginot et al., 2019). Almost half of the ice sheet mass loss occurs at marine-terminating outlet glaciers (Enderlin et al., 2014; IMBIE Team, 2019; Mankoff et al., 2020; Mouginot et al., 2019; van den Broeke et al., 2009) and changes in total ice sheet discharge appear to be related to shifts in outlet glacier frontal position (King et al., 2018, 2020). Enhanced submarine melting driven by ocean warming has been implicated in many recent glacier front retreat events (Millan et al., 2018; Walsh et al., 2012), such as at Jakobshavn Isbrae (Holland et al., 2008), Zachariae Isstrom (Mouginot et al., 2015), Kangerdlugssuaq (Bevan et al., 2019; Christoffersen et al., 2011; Inall et al., 2014), and Helheim Glacier (Howat et al., 2008). These glaciers alone accounted for more than 40% of Greenland's ice discharge change, as opposed to surface runoff, between 2000 and 2012 (Enderlin et al., 2014). However, the changes in ocean circulation that may have led to these glacier retreat events are weakly characterized. Changes in ocean temperature and volume transport near Greenland's tidewater systems were mostly unmonitored during many earlier events.

Sermilik Fjord abuts Helheim Glacier, one of Greenland's largest glaciers (Enderlin et al., 2014; Rignot & Kanagaratnam, 2006). The region is among the best instrumented and understood glacier-ocean systems (Straneo et al., 2016), making it an ideal area to investigate the extent to which remotely sensed sea surface temperature (SST) variability may be used to infer ocean variability in the vicinity of an outlet glacier, where oceanographic thermal characteristics can be of great significance. The ocean circulation and heat transport within the fjord and on the continental shelf is highly variable (Jackson et al., 2014; Straneo et al., 2010; Sutherland et al., 2013). Heat is primarily carried by relatively warm, saline Atlantic Water (AW; ~2.0°–5.2°C, deeper than 150–250 m) from the Irminger Current (IC) that circulates offshore of the continental shelf break (Jackson et al., 2014; Straneo et al., 2010). The IC carries AW equatorwards at the surface and extending down to depths greater than 500 m (Andresen et al., 2012; Johannessen et al., 2011; Rudels et al., 2002; Våge et al., 2011). Along the inner shelf, the East Greenland Coastal Current (EGCC) is a low salinity wedge perched atop deeper AW (Bacon et al., 2002; Sutherland & Pickart, 2008). Above 150–250 m, the upper layer carries cold and fresh Polar Water (PW; <4°C). The EGCC flows south, 20–30 km wide, hugging the Greenland coastline (Sutherland & Pickart, 2008). Transport within the EGCC varies seasonally with the greatest freshwater transport in December and higher transport in winter and spring coinciding with its speedup and deepening (Bacon et al., 2014; Harden et al., 2014; Le Bras et al., 2018; Straneo et al., 2010; Sutherland & Pickart, 2008). Freshwater within the EGCC derives primarily from export out of the Arctic, via Fram Strait, with relatively small, highly diluted contributions from the eastern Greenland fjords (Bacon et al., 2002; Harden et al., 2014; Sutherland & Pickart, 2008), including Sermilik which contributes ~1.4% of the EGCC's freshwater content (Beaird et al., 2018). From summer shipboard surveys and longer term mooring deployments, research in this area has suggested that seasonality in EGCC width, depth, and transport along the shelf is controlled by alongshore winds (Harden et al., 2014; Le Bras et al., 2018; Sutherland & Pickart, 2008). IC and EGCC variability on the shelf can influence water properties in Sermilik Fjord and therefore, the glacier front; however, ocean variability on the shelf and within the fjord is largely unknown before the record began in 2008 (Straneo et al., 2016), years after the first records of thinning and retreat at Helheim Glacier (Howat et al., 2005; Luckman et al., 2006).

While the EGCC and IC have been relatively well studied, the interactions between them in the region outside of Sermilik Fjord, and the temporal variability in those interactions, are poorly understood as a result of limited spatial and temporal measurement coverage. Warm AW encroaches onto most of the shelf below PW throughout the year, often via troughs that cut across the continental shelf and into the fjords at depth (Rudels et al., 2002; Sutherland et al., 2013). The AW near the coast is cooler than at the shelf break as a result of surface cooling and mixing with PW (Straneo et al., 2012). Farther from the coast, AW can flow onto the shelf as full-depth occasional intrusions within the troughs or seasonally varying inflow across portions of the shelf (Harden et al., 2014; Sutherland et al., 2013). This seasonal inflow intensifies in the fall and is associated with a narrower EGCC banked up against the coast (Harden et al., 2014). More frequent AW intrusions may lead to warmer waters on the inner shelf (Straneo & Heimbach, 2013), with greater influence of AW on the shelf linked to increased glacier calving activity (Andresen et al., 2012). All past oceanographic work in this region is limited spatially or temporally relative to the scale of the continental shelf, which extends ~200 km out from the coast. As a result, little is known about the variability of the AW across much of the shelf and its influence on inner shelf and fjord water temperatures. However, research does clearly show

that AW inflow and therefore, heat transport onto the shelf (Harden et al., 2014; Sutherland et al., 2013) and into the fjord (Jackson et al., 2014; Straneo et al., 2010) varies substantially over short and long timescales.

The availability of remotely sensed SST records from the period prior to the speedup of many Greenland glaciers that occurred in the early 2000s raises the possibility of inferring oceanic variability at Greenland's glacial margins through proxies that are built on SSTs. SST depends strongly on the depth, magnitude, and history of thermal gradients and stratification at the surface (Donlon et al., 2002, see Figure S1). These properties are controlled by solar heating, heat exchange with the atmosphere, and heat exchange with deeper waters (e.g., Donlon et al., 2002; Minnett, 2003). SST will therefore be impacted by, and potentially covary with, both atmospheric and ocean mixed layer temperature changes (e.g., Frankignoul & Hasselmann, 1977; Jaswal et al., 2012). Several recent studies have attempted to define SST-ocean temperature relations largely through comparisons between glacier activity and SST variability with differing results (Andresen et al., 2012; Howat et al., 2008, 2010; Khan et al., 2014; Schild & Hamilton, 2013). Those studies largely do not address the physics relating SSTs to deeper water temperatures, therefore, important questions remain about the extent to which SSTs around Greenland provide information about the subsurface water column (below 150–250 m) where the AW, which influences submarine melting of the larger glaciers, resides. Important progress has been made by Sutherland et al. (2013) who found that, for the period from 2004 to 2010, summertime (June, July, August) MODerate resolution Imaging Spectroradiometer (MODIS) SSTs on the continental shelf near Sermilik Fjord correlated closely with tagged-seal temperature measurements at 50 m depth, with diminishing correlation at deeper depths until decoupling below 250 m. However, a broader treatment is necessary in order to constrain temporal variations in ocean temperatures, which is crucial for discerning ice-ocean interactions in glacier retreat events back through time.

Here, we investigate the use of SSTs as a means to assess the variability of the surface and subsurface waters that enter Greenland's glacial fjords and melt glaciers at depth (Straneo et al., 2012). In contrast to other studies, we make use of oceanographic subsurface data to investigate the correlation between surface properties in different regions on the shelf, in the vicinity of Sermilik Fjord, and those observed at depth at the mouth of the fjord. In Section 2, we describe the data sets and methods used in this study. We then describe the variability in the SST records and examine the relationships between SSTs and the atmospheric and ocean temperature variability that contributes to it in Section 3. Using these relationships, we estimate upper ocean temperatures and derive a proxy for subsurface AW temperatures from SSTs adjusted for local air temperatures to produce the first AW record near Sermilik Fjord dating back to 2000. We also track AW intrusion variability along the trough leading to Sermilik Fjord to give insight into the drivers of subsurface AW temperature changes on the shelf. In Section 4, we further discuss the utility of SSTs and their caveats, and the implications of the subsurface AW record we have derived within the backdrop of the Helheim Glacier and broader southeastern Greenland systems. While our findings and this method are specific to the oceanography of this region, our analysis demonstrates that SSTs provide novel insight into ocean variability around Greenland, which is crucial for identifying glacier-ocean processes and glacier retreat attribution.

2. Data and Methods

2.1. Satellite-Derived Sea Surface Temperatures

In contrast to in situ data, SSTs acquired from satellites offer broader spatial and temporal records for tracking ocean temperature and extent of AW inflow onto the continental shelf. To help reconstruct ocean variability here, we use MODIS-derived SSTs, which provide the temperatures of the ocean skin (upper few μm; SST_{skin}; see Figure S1; Donlon et al., 2002). The accessibility of MODIS SST products, the instrument's moderate spatial resolution, and its ~15 scans per day by each of the two satellites on which it flies (Aqua and Terra) provide extensive spatiotemporal coverage suitable for our objectives. In this work we use the MODIS Aqua and Terra daily global level 3 4-km mapped thermal daytime and nighttime SST V2014.0 products (quality level 0 and 1) derived from the 11 and 12 μm thermal infrared channels 31 and 32, respectively (Kilpatrick et al., 2015; Ocean Biology Processing Group, O. E. L. and NASA Goddard Space Flight Center, 2014a, 2014b). The data we use span the period beginning February 24, 2000 for Terra and July 4, 2002 for Aqua, and ending December 31, 2018 for both satellites. The retrieval error for the SSTs is ~0.4°C (Kilpatrick et al., 2015). We reference the four MODIS SST products hereafter based on their division

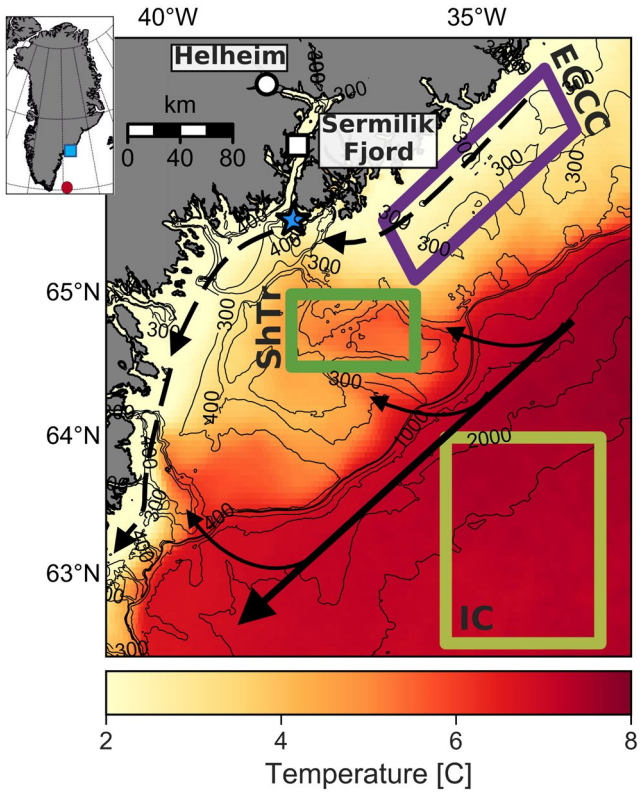

Figure 1. 2000–2016 mean nighttime MODerate resolution Imaging Spectroradiometer (MODIS) sea surface temperature (SST) of the Ammassalik region around Sermilik Fjord. Solid black arrows show the location of the Irminger Current (IC) and dashed show the East Greenland Coastal Current (EGCC), which mix across the Shelf Trough (ShTr) region. Boxes indicate areas over which SST is averaged for each region, the blue star shows the fjord mouth mooring, the red circle gives the location of the Ocean Observatories Initiative (OOI) mooring, the white circle marks Helheim Glacier front, and white square is in Sermilik Fjord. Bathymetry from BedMachine v3 is in thin black lines at 300, 400, 500 m, and every 500 m thereafter (Morlighem et al., 2017).

by satellite and time of day: Terra daytime (T-D), Terra nighttime (T-N), Aqua daytime (A-D), and Aqua nighttime (A-N).

Before extracting SSTs from each of the four products, we account for cloud and sea ice contamination that may occur because the MODIS SST processing pipelines are not optimized for polar climates (Jia & Minnett, 2020; Kilpatrick et al., 2019; see supporting information). Arctic SSTs can have cloud contamination (Kilpatrick et al., 2019) that introduces noise by shifting SST retrievals toward an artificially cold measurement (Ackerman et al., 1998). To reduce these effects, we apply spatial and temporal averaging for each sampling region and across multiple SST products, as described below. Sea ice contamination can also lead to a cool bias in the SST retrievals, and we find that the daytime SST products, especially in Aqua, contain systematically more sea ice contamination (Figure S2a). To reduce sea ice misclassification and these inter-product differences, we apply a separate sea ice mask, created from MODIS and passive microwave sea ice products, to the four daily SST products (see Supplementary Information).

2.2. Sampling Regions

To investigate SST spatial and temporal variability near Sermilik Fjord, we examine three regions: the IC, the EGCC, and the Shelf Trough (ShTr) regions (Figure 1). We chose the IC and EGCC sampling regions based on the observations from Rudels et al. (2002) and Sutherland and Pickart (2008) that characterize the locations of the respective currents, and chose the box sizes to include relatively homogeneous SSTs based on the SST climatology from the region. We use IC and EGCC regions as indicative of AW and PW end members, respectively, because these are the primary water masses at the surface in the respective boxes (Rudels et al., 2002; Sutherland et al., 2013). In addition, we define a "ShTr region" over the trough leading to Sermilik Fjord, where AW flows onto the shelf and mixes with the PW of the EGCC (Sutherland et al., 2013). Results for the ShTr are not sensitive to small changes in the box locations and size (Figure S3; Table S1; see supporting information).

2.3. Seasonal and Diurnal Biases

Seasonal differences in instrument scan coverage between the Level 3 MODIS SST products must be accounted for before they are used to investigate ocean variability in polar regions. Each MODIS instrument acquires 12–18 scans of our study region each day. During the summer solstice, few are classified as nighttime and most scans are binned into the daytime product (Figure S2b). The opposite is true during the winter solstice. As there is a far higher likelihood of getting at least one sea ice- and cloud-free measurement during a day with more scans, this disparity in scan coverage between seasons indicates that the daytime products (daily, 8-day, monthly, annual) are skewed to summer measurements and nighttime toward winter. As a result of these differences, creating a robust and continuous record of SSTs that is representative of all seasons requires creating a composite by combining day- and nighttime SSTs for each region.

The day- and nighttime products carry inherent biases based on diurnal differences in values of SST_{skin}, which we remove before combining the data sets into a daily composite. Diurnal biases cause a decoupling between the ocean skin and underlying water (Donlon et al., 2002; Minnett, 2003; Price et al., 1986). They are expected as a result of differences in diurnal thermocline and skin temperature effects on SST_{skin} between day- and nighttime, which also vary seasonally (e.g., Eastwood et al., 2011; Koizumi, 1956; Sverdrup et al., 1942). We calculate the diurnal bias based on differences between the day- and nighttime products for

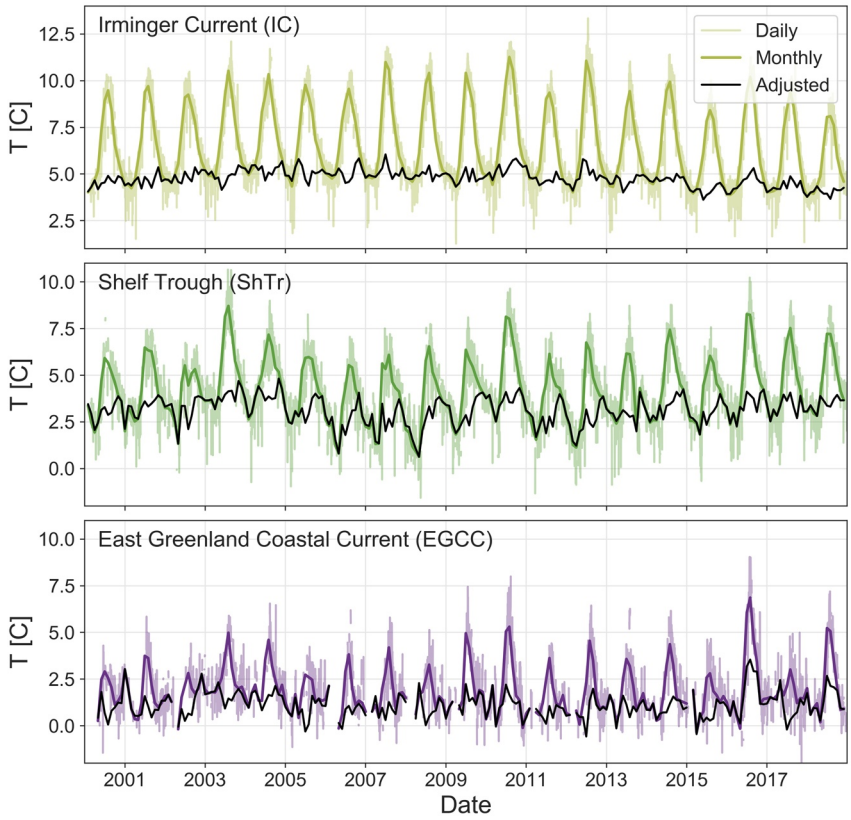

Figure 2. Composite and adjusted *SST* records for each sampling area. Monthly mean (thick) and daily (thin) *SST* composite records for the IC (yellow), ShTr (green), and EGCC (purple) boxes are shown. The *SST* adjusted for air temperature is shown as black lines (see Section 3.3 for description). EGCC, East Greenland Coastal Current; IC, Irminger Current; ShTr, Shelf Trough; SST, sea surface temperature.

each region separately. To determine the biases, we first take the mean of the pixels in the sampling boxes and produce daily time series from 2000 to 2018 for each of the four masked daily products (Figure 1). We average the A-D and T-D products together to produce a daytime average for each region. We do the same for the two nighttime products. From these records, we produce a day- and nighttime climatology for each of the sampling regions using monthly means across the entire 19-year record (Figure S4, see supporting information). We calculate standard error for the climatologies between the 19 years of monthly data. We define the seasonally varying diurnal bias as the systematic warm bias in the daytime products in comparison to the nighttime records across the climatologies (on average 0.28 ± 0.15°, 0.39 ± 0.16°, 0.46 ± 0.23°C for the IC, ShTr, and available EGCC time period, respectively; see supporting information). We use the seasonally varying diurnal biases for each sampling location – which result from wind speed and solar radiative forcing (Kawai & Wada, 2007) – and subtract them from the daytime product.

With the diurnal bias removed from the daytime records so that they are equivalent to the nighttime, we assume that all four records represent the bulk SST temperature (Figure S1; Sutherland et al., 2013) and that they can be combined into a composite record. This assumption for nighttime SST_{skin} is consistent with Minnett (2003) and used by others (e.g., Jia & Minnett, 2020; Kilpatrick et al., 2015). We hereafter refer to this bulk temperature as *SST*, although the measurement will also still contain a slight and constant cool skin bias to bulk temperatures as a result of heat flux to the atmosphere (~0.17°C; Donlon et al., 2002). We average the nighttime and corrected daytime records to produce the composite daily *SST* time series for each region (Figures 2 and S4). The daily time series includes some noise from cloud contamination and the daily record during multiple months of the year can include only one or two measurements per week as a result of high cloud cover. Therefore, to reduce the impact of cloud contamination on the record, we also aggregate daily measurements to produce weekly and monthly mean SST time series for our analyses.

2.4. Air and Ocean Temperature Records

To determine the extent to which variability in satellite-derived *SST* can be used to reconstruct upper ocean (surface mixed layer) temperature outside Sermilik Fjord, we consider two factors that influence *SST* variability: (1) air and (2) ocean temperatures. We use the European Center Medium-Range Weather Forecasts (ECMWF) ERA-5 operational reanalysis data set (Copernicus Climate Change Service, 2017; Hersbach et al., 2020) to assess the relationships between *SST* and air temperatures in each region. From ERA-5, we use the 2-m air temperature measured at 6-hourly intervals on a 0.5° × 0.5° grid. Air temperatures vary significantly across our study region and are, thus, averaged to daily time steps for each of the *SST* sampling areas, separately.

The water column in the IC and ShTr regions can be relatively homogeneous from surface to depth, the latter as a result of full-depth AW layers flowing from the IC onto the shelf along the trough (Harden et al., 2014; Sutherland et al., 2013). Therefore, we use surface and subsurface ocean temperatures from these locations for comparison to *SST*. We use the Ocean Observatories Initiative (OOI) Flanking Mooring A Microcat SBE37 temperature record from 180 m deep in the Irminger Gyre for comparison to the IC *SST*. This OOI mooring sits offshore (south) of the IC box (Figure 1) and shares similar water properties (Krauss, 1995; Våge et al., 2011). The OOI record we use spans September 9, 2014 – December 31, 2018 collected at 7.5 min intervals. We refer to this mooring as the OOI mooring, hereafter. We determine subsurface water temperature variability on the inner shelf below the EGCC using data from a mooring deployed multiple times between August 24, 2009 and August 18, 2013 on the continental shelf within the trough that leads to Sermilik Fjord (see Figure 1 for location; Harden et al., 2014; Jackson & Straneo, 2016; Jackson et al., 2014). From this mooring – referred to as the "fjord mouth" mooring – we use the temperatures recorded by one instrument each year, either a Microcat SBE37SM or XR 420 RBR sensor, deployed between 262 and 305 m. The fjord mouth moorings recorded temperatures every 7.5–15 min. In processing, the records were calibrated at release and retrieval and then despiked. The fjord mouth mooring temperatures provide a time-varying record of subsurface AW that is known to flow into Sermilik Fjord (Jackson & Straneo, 2016; Straneo et al., 2011). Both the OOI and fjord mouth mooring records are averaged to daily intervals.

3. Results

3.1. Seasonal and Interannual

In this work, we examine the seasonal and interannual variability of the water properties reaching Sermilik Fjord and their relationships to the SST-derived properties in the ShTr and the two regions feeding the ShTr. Across the 19-year record, the IC is warmest on average (6.5 ± 0.6°C) and the EGCC coolest (2.3 ± 0.3°C), with ShTr temperatures between them (4.3 ± 0.4°C), which is consistent with the ShTr being a mixing region for AW and PW (Sutherland et al., 2013). Similarly, the IC has the largest seasonal range (5.3°C), with the ShTr and EGCC having progressively smaller ranges (4.3°C and 3.3°C, respectively; see supporting information). Across the entire record, the seasonal cycle dominates the interannual variability for the three regions, especially for the IC and ShTr (Figure 2), and the interannual variability of the EGCC is more prominent because the EGCC has a smaller seasonal signal.

3.2. Dependence on Air Temperature

To determine the extent to which air temperature controls *SST* variability near Sermilik Fjord, we compare the *SST* with ERA-5 air temperature records (Figures 3 and S5). We use ordinary least squares (OLS) regression to examine the linear relationships between air temperature and *SST* in each of the regions separately (Seabold & Perktold, 2010). We test these relationships for daily, weekly, and monthly timescales and determine that the daily averaging window has the most consistent variability between regions (Figure S6; see supporting information). We, therefore, use daily averages in the regression herein.

Using the OLS regression model, we find that daily *SST* in all regions have a strong linear relationship with ERA-5 air temperature records in summer, but that this relationship does not hold in winter (Figure 3; Table 1). For example, ShTr *SST* has the strongest linear relationship ($r^2 = 0.44$, $p < 0.001$) with daily air temperatures in summer (June, July, August, September; slope = 0.61 ± 0.03; Figure S5b), but the relationship

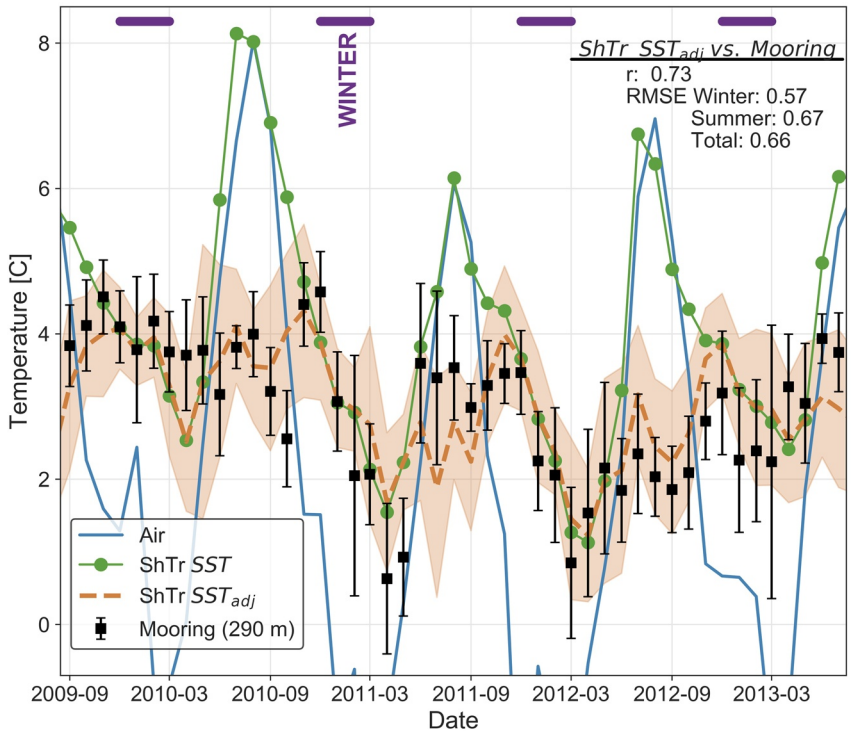

Figure 3. The Shelf Trough (ShTr) bulk sea surface temperature *(SST)* compared to other temperature records. Monthly ShTr *SST* (green) are compared to air temperatures (blue) and fjord mouth mooring water temperatures from 290 m (black). We also show the SST_{adj} (orange) derived in Section 3.3 – which we identify as a fjord mouth subsurface temperature proxy. The root mean square error (RMSE) between SST_{adj} and mooring temperature records are given. Standard deviations for the ShTr adjusted *SST* (SST_{adj}) and mooring temperatures are shown as orange shading and error bars, respectively. Winter (purple) months are shown. Not shown, air temperature reaches −1° to −6°C each winter.

becomes weak or insignificant ($r^2 = 0.03$, $p < 0.001$) during winter months (December, January, February, March; slope = 0.06 ± 0.02). For the remaining months (Apr, May, Oct, Nov), *SST* shows a weaker correlation with air temperature (slope = 0.31 ± 0.03; $r^2 = 0.19$, $p < 0.001$). Our findings are consistent with a shallower mixed layer or strongly stratified surface ocean in non-winter months, which results in a more closely coupled air-sea temperature response than in winter (Chang, 1993). It is also consistent with previous work that found a weaker coupling between *SST* and air temperature in winter than in summer around Greenland (Singh et al., 2005, 2006). This seasonality in the relationships holds for all three sampling regions with the ShTr experiencing the strongest air-SST coupling and the weakest ones in the EGCC. However, the significance of the relationships in some months differ slightly (Figure S6; see Section 3.3). This is expected based on stratification and heating differences between the regions (e.g., Sutherland & Pickart, 2008), which affect ocean skin temperatures and air-sea interactions (Garwood, 1979).

3.3. Upper Ocean Temperatures

Since *SST* can have a strong linear relationship with air temperature in non-winter months (proportionality as large as 0.6; Table 1), consistent with a stronger near-surface stratification, we removed the portion of *SST* variability related to air temperature to obtain a better indicator of upper ocean layer temperatures. To do this, we build a multivariate linear model that expresses daily *SST* for each region as the combination of a portion that covaries with air (T_{air}) and one that covaries with upper ocean (T_{ocean}) temperatures:

$$SST(R,t) = \mathrm{A_m}(R)\mathrm{T_{air}}(R,t) + \mathrm{B}(R)\mathrm{T_{ocean}}(R,t) + \mathrm{C}(R) \quad (1)$$

where A_m is the proportionality coefficient for the relationship between *SST* and air temperature that varies by month (indicated by the subscript m), B is a constant proportionality coefficient with upper ocean

Table 1
A_m Parameters Calculated by the Ordinary Least Squares Regression Models for the ShTr, IC, and EGCC

	ShTr	IC	EGCC
	$N = 4{,}587$	$N = 5{,}747$	$N = 2{,}960$
Month	$R^2 = 0.62$	$R^2 = 0.84$	$R^2 = 0.52$
Jan	**0.04 ± 0.04**	−0.02 ± 0.03	**−0.07 ± 0.05**
Feb	**0.05 ± 0.04**	**−0.03 ± 0.03**	−0.04 ± 0.08
Mar	**0.11 ± 0.04**	**−0.07 ± 0.03**	−0.06 ± 0.06
Apr	**0.10 ± 0.06**	0.00 ± 0.02	**−0.16 ± 0.14**
May	0.06 ± 0.06	**0.21 ± 0.02**	**−0.13 ± 0.09**
Jun	**0.47 ± 0.04**	**0.42 ± 0.01**	**0.19 ± 0.04**
Jul	**0.60 ± 0.02**	**0.52 ± 0.01**	**0.42 ± 0.02**
Aug	**0.56 ± 0.02**	**0.52 ± 0.01**	**0.46 ± 0.02**
Sep	**0.50 ± 0.02**	**0.48 ± 0.01**	**0.33 ± 0.03**
Oct	**0.50 ± 0.04**	**0.39 ± 0.01**	**0.15 ± 0.04**
Nov	**0.28 ± 0.05**	**0.24 ± 0.02**	**−0.07 ± 0.05**
Dec	0.00 ± 0.04	**0.09 ± 0.02**	**−0.13 ± 0.04**

Standard error is given for each parameter. Number of measurements (N) and R^2 provided for each model. Intercept and insignificant parameters not used for corrections.

Abbreviations: EGCC, East Greenland Coastal Current; IC, Irminger Current; ShTr, Shelf Trough.

Bold indicates parameters significantly different than zero ($p \leq 0.05$).

temperatures, and C is a skin bias (expected to be similar to the ∼−0.17 global average; Donlon et al., 2002). We assume that this relationship holds for each of the regions with coefficients that are region (R) and time (t) dependent. Physically, $A_m T_{air}(t)$ represents the variability resulting from air-sea interactions, which is a function of the heat exchange between the near-surface ocean layers (dependent on layer thickness), the short and longer term flux of latent and sensible heat through the air-sea interface (dependent on air temperature, ocean temperature, wind speed, and humidity), short- and long-wave radiation through the ocean surface, salinity effects, and horizontal advection (Denman, 1973; Frankignoul & Hasselmann, 1977; Kraus & Turner, 1967). Previous climate modeling work has estimated the linkage between air temperature and *SST*, sometimes using a simple bias correction (Schulz et al., 1997) or through more complex relationships that include humidity and wind speed (Gautier et al., 1998; Jones et al., 1999; Konda et al., 1996; Singh et al., 2006). The relationship between air temperatures and *SST* is complex but, as we show in Section 4.2 and below, it can be approximated in our study regions as a simple statistical linear relationship. We use monthly coefficients, which is common for SST corrections, especially those tied to solar radiation and seasonality (e.g., Kilpatrick et al., 2015). For each region (R), we further define an adjusted *SST* (SST_{adj}):

$$SST_{adj}(R,t) = SST(R,t) - \mathrm{A_m}(R)\mathrm{T_{air}}(R,t) \quad (2)$$

where $A_m T_{air}(t)$ is subtracted to remove the *SST* variability tied to the atmosphere. We calculate A_m for each region, and each month, using an OLS regression model with a monthly interaction term that finds the seasonally varying slope relationships between daily *SST* and air temperatures (Table 1). For months with statistically insignificant slope relationships ($p > 0.05$), we apply $A = 0$; therefore, SST_{adj} is equivalent to *SST* for some winter and spring months.

The SST_{adj} for the three regions have a wide range of seasonal and interannual variability that represents the upper ocean temperature variability (Figure S1). We confirm that the SST_{adj} represent the upper ocean waters using the OOI mooring record for comparison to the IC (Figure 4). Despite a distance of 445 km between the center of the IC box and the OOI mooring, the IC SST_{adj} significantly correlates ($r = 0.32$, $p = 0.02$) with the temperature record from 180 m deep. This agrees with previous work showing that the water in the IC is relatively homogeneous throughout the surface water column and often has a mixed layer deeper than 180 m (de Jong et al., 2018). While we do not have a surface mooring record from within the EGCC, the EGCC and IC monthly and interannual SST_{adj} variability (Figure 4) is consistent with ranges in the upper ocean mooring temperatures described by Harden et al. (2014). We describe ShTr SST_{adj} linkages to subsurface waters below. When we compare the three upper ocean records, we find that, unlike the absolute *SST*, the ShTr SST_{adj} exhibit a larger seasonal range (1.7°C) than the EGCC and IC (0.6° and 0.4°C, respectively). This is consistent with synoptic and seasonal upper ocean temperature swings associated with seasonal heating cycles, cold meltwater influx, and variable AW inflow inshore (Harden et al., 2014; Straneo et al., 2010). SST_{adj} temperature ranges are ∼2°–5°C smaller than those of the absolute *SST* (Figure 2), which is consistent with differences between upper ocean temperatures and bulk *SST* (see Figure S1; Chang, 1993).

Using a second-order low-pass digital Butterworth Filter (Virtanen et al., 2019), with a 24-month cutoff frequency, we further examine the longer term SST_{adj} records for the three different regions. While we find that the smoothed upper ocean records were warmest in the early 2000s in all three regions, the records diverged in subsequent years. Specifically, the IC remained warm from 2005 to 2008, while the ShTr and EGCC experienced cooling that was more pronounced for the ShTr than the EGCC. Furthermore, the ShTr box also continuously warmed after 2012, whereas the IC exhibited long-term cooling, consistent with the deepening of convection in the Irminger Sea and generalized cooling of the subpolar gyre during this period

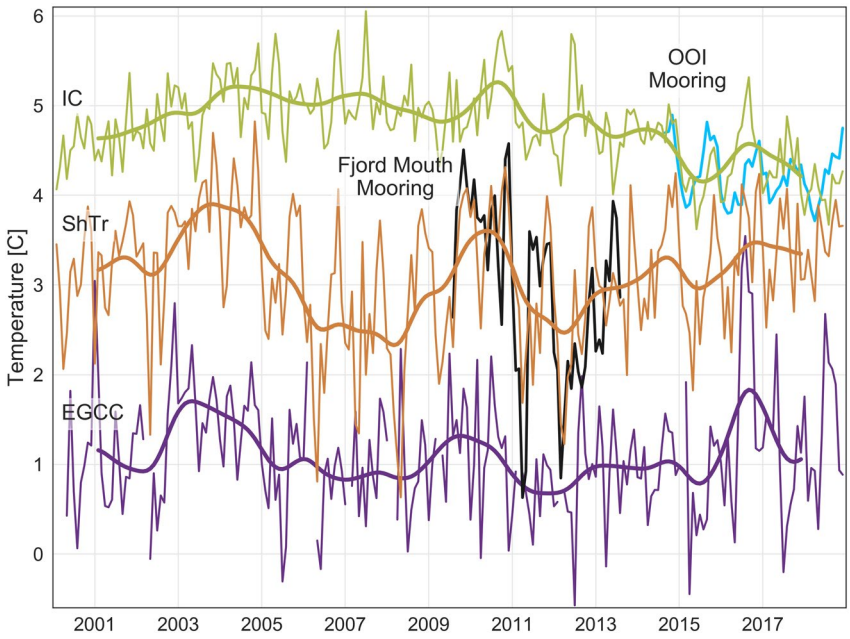

Figure 4. Monthly adjusted sea surface temperature (SST_{adj}) records for 2000–2018 for the Irminger Current (IC; green), Shelf Trough (ShTr; orange), and East Greenland Coastal Current (EGCC; purple). Thin lines are monthly *SST* while thick lines represent 24- month low-pass Butterworth filtered records for each. The fjord mouth (290 m: Black) and Ocean Observatories Initiative (OOI) mooring temperatures (180 m; blue) are shown for comparison. The ShTr SST_{adj} record is a proxy for the fjord mouth mooring temperatures.

(de Jong & Steur, 2016; de Jong et al., 2018). Over the 19-year record, warmer years in the ShTr record were consistent with IC temperatures, while they more closely resembled EGCC temperatures in the coldest years. Although the upper ocean temperature records for the three regions differed substantially, ShTr SST_{adj} correlated more with the EGCC ($r = 0.34$, $p < 0.001$) than the IC ($r = 0.16$, $p = 0.01$). We further explain reasons for these relationships in Sections 3.5 and 4.2.

3.4. *SST* on the Shelf and a Fjord Mouth Subsurface Water Temperature Proxy

We investigate the connection between ShTr *SST* and the fjord mouth subsurface mooring temperatures using the OLS regression model. The ShTr box is a region where AW inflow can extend all the way to the surface (Sutherland et al., 2013). In the regression, we use daily, weekly, and monthly averages to test the most appropriate timescale for comparisons between *SST* and mooring temperatures (Figure 5). We find that ShTr *SST* relates linearly with subsurface water temperatures for all three averaging windows in wintertime only, and the monthly data yield the strongest and most significant regressions. Specifically, monthly fjord mouth mooring temperatures (290 m) have a significant linear relationship with ShTr *SST* in winter (slope = 1.18 ± 0.35, $r^2 = 0.79$, $p < 0.001$), but not in summer months (slope = 0.18 ± 0.29, $r^2 = 0.10$, $p = 0.206$; Figure 5c). Markedly, the strong relationship between ShTr *SST* and subsurface waters occurs in the months when *SST* shows little linkage to air temperature and the region receives little solar insolation.

We attribute this relationship to linkage between the upper ocean water masses in the ShTr box and those found subsurface at the fjord mouth mooring location further downstream. This relationship is consistent with the results of Sutherland et al. (2013), who showed that full-depth AW intrusions occur in the ShTr region and that AW are found subsurface at the mooring. Conversely, surface waters at the mooring location are indicative of PW properties, consistent with the stratification described by Harden et al. (2014). Based on observed along-trough velocities of 0.0–0.6 ms^{-1} (Harden et al., 2014; Sutherland & Pickart, 2008) and wind-driven velocity shifts on synoptic timescales (Jackson et al., 2014), we expect a temperature lag for water transport between the middle of the ShTr box and the mooring site (~80 km) that may range from a day to more than a week – supporting our choice to focus on monthly variability. The stronger wintertime

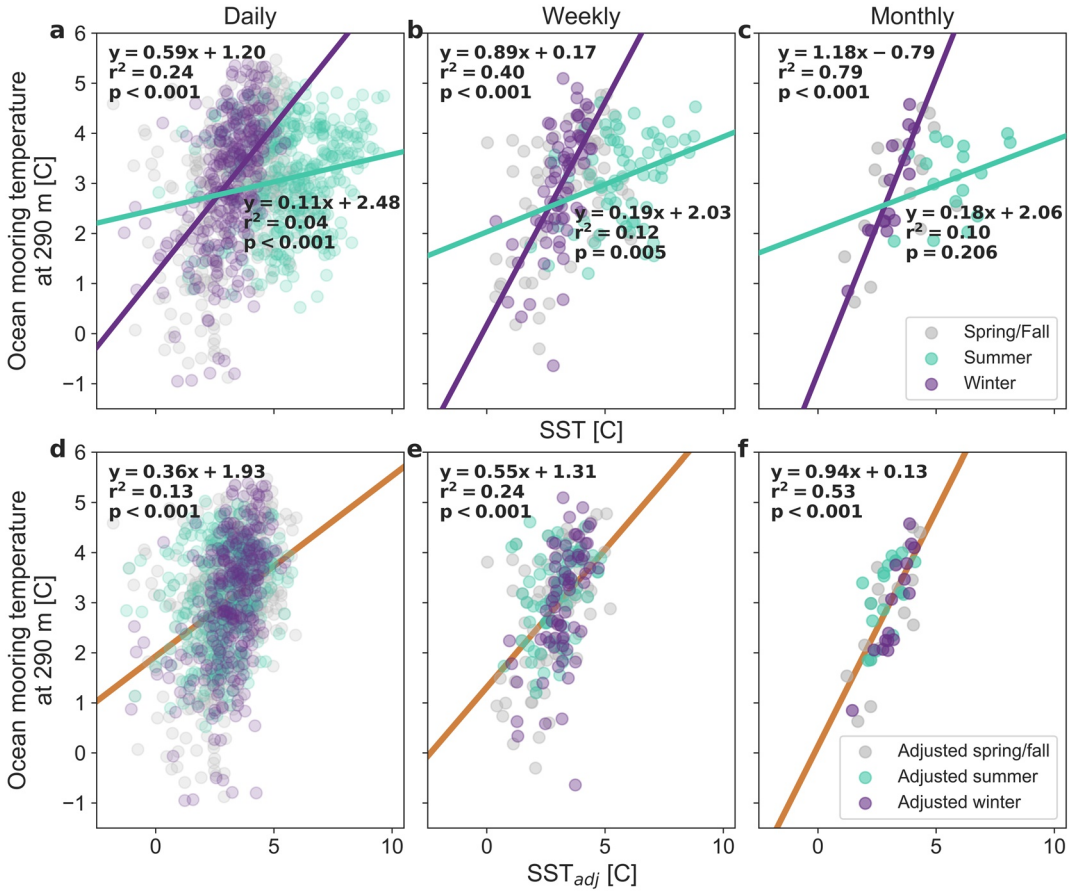

Figure 5. Seasonal correspondence between fjord mouth mooring temperatures and Shelf Trough sea surface temperature *(SST)* before and after air temperature correction using (a, d) daily, (b, e) weekly, and (c, f) monthly mean temperatures. (a, b, and c) Linear relationships between daily mooring temperatures from 290 m near the mouth of Sermilik Fjord and Shelf Trough SST for winter (purple), summer (teal), and spring and fall (gray). Equations with r^2 and p-values are given for winter (top of each panel) and summer (bottom). (d, e, and f) Mooring temperatures versus the new SST adjusted by air temperatures (SST_{adj}). The trend line (orange) and equation for all seasons is shown.

mooring/*SST* relationship is consistent with deepening of the IC wintertime mixed layer as a result of air-sea forcing (de Jong et al., 2018; Våge et al., 2011).

We also test the extent to which the new ShTr SST_{adj} resembles the subsurface water temperatures at depth at the mooring location near Sermilik Fjord mouth and find good agreement between the records. The ocean mooring temperatures have a positive linear relationship with ShTr SST_{adj} (slope = 0.94 ± 0.26, $r^2 = 0.53$, $p < 0.001$; Figure 5) that is similar to the wintertime relationship (slope = 1.18 ± 0.35) found using the bulk *SST*. Further, we find a strong correlation ($r = 0.73$, $p < 0.001$) between ShTr SST_{adj} and mooring temperatures that is also stronger for wintertime measurements (Figure 3; winter RMSE = 0.57°C, summer RMSE = 0.67°C, total RMSE = 0.66°C).

In addition to the correspondence between the mooring data and the SST_{adj} in the ShTr region, the fact that the ShTr SST_{adj} is warmest in November and December and coolest from March to May (Figure S7) is consistent with subsurface temperatures observed on the shelf between 2004 and 2010 using tagged seals (Straneo et al., 2010). We also find good relative agreement between ShTr SST_{adj} measurements and shipboard hydrographic surveys within the trough taken each August from 2009 to 2013 (Harden et al., 2014). This indicates that the monthly ShTr SST_{adj} derived here is a useful proxy for the subsurface ocean temperatures at the fjord mouth and hence of the waters that feed Sermilik Fjord at depth and reach the base of Helheim Glacier (Straneo et al., 2010).

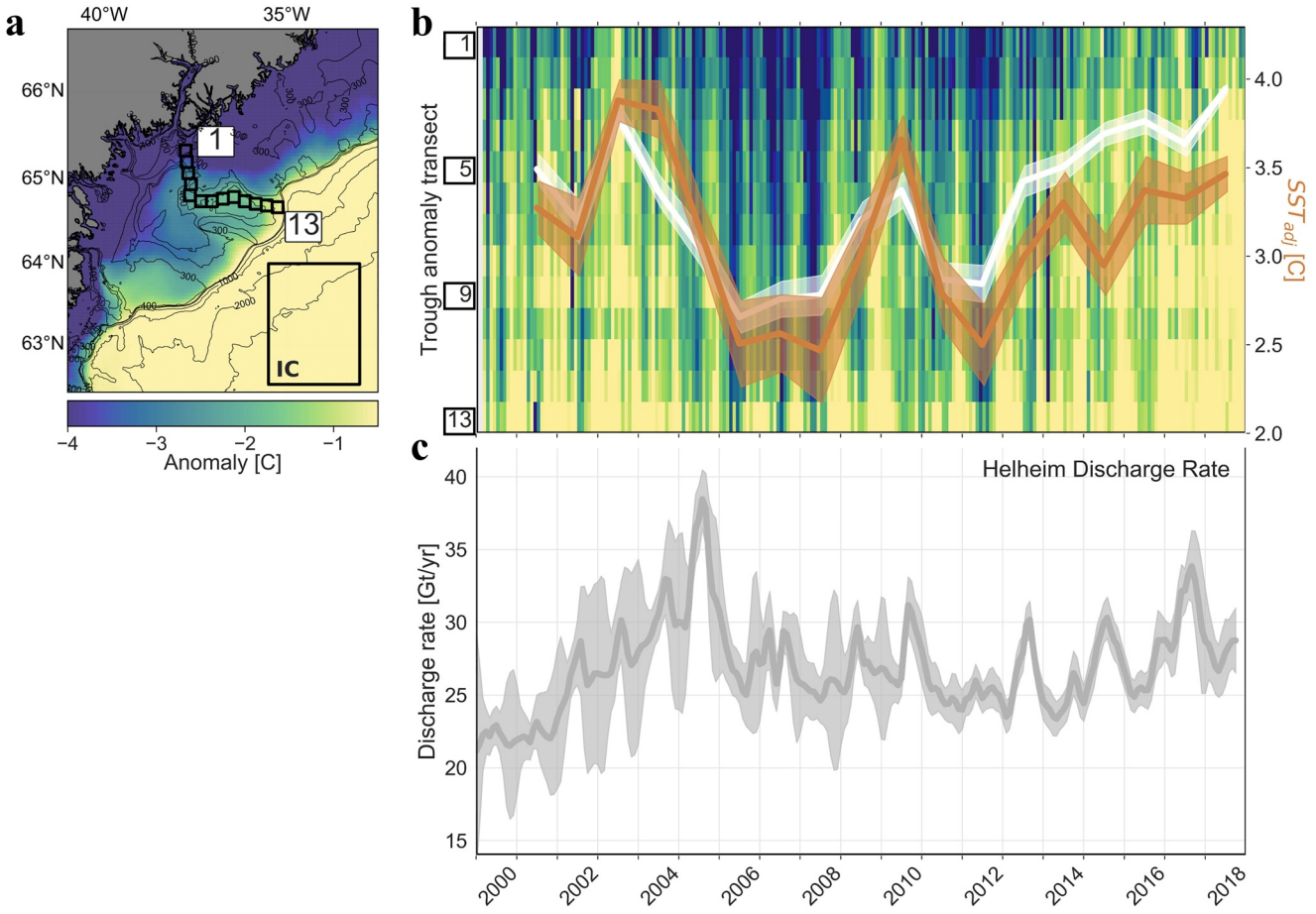

Figure 6. Variability in the trough anomaly along the trough leading to Sermilik Fjord in comparison to Helheim Glacier discharge rates. (a) Map of the 19-year climatological anomaly of adjusted sea surface temperature (SST_{adj}) overlain by the thirteen – 14 × 14 km sampling boxes representing a transect from the fjord (1) out to the continental slope (13). Bathymetry contours from BedMachine v3 (Morlighem et al., 2017). (b) Monthly record for the trough anomaly from 2000 to 2018. The transect from box (1) on the top to (13) at the bottom spans the *y*-axis, and time is along the *x*-axis. The annual means for the −1.5°C trough anomaly (white; spatial indicator of a temperature contour on the shelf) and Shelf Trough (ShTr) SST_{adj} (orange; a temperature indicator from the fixed ShTr box) are shown with standard error (shading). (c) Monthly Helheim Glacier ice discharge rates and their standard error from King et al. (2020) to provide a comparison between Helheim Glacier changes and ocean records from (b).

3.5. AW Encroachment Onto the Shelf

Temperature changes in the ShTr region, which is a mixing region between AW and PW at the surface (Harden et al., 2014; Sutherland et al., 2013), reflect the combined influence of IC and EGCC temperature variability and transport between them. Here, we investigate changes in the AW intrusions onto the continental shelf by examining the occurrence of warm temperatures along the trough that supplies AW to the ShTr region and eventually, at depth, to Sermilik Fjord (Figure 6). Specifically, we consider a transect of thirteen 14 × 14 km boxes along the trough crossing the continental shelf and leading to Sermilik Fjord. Within each of the boxes we subtract the daily IC SST_{adj} temperature from the SST_{adj} in the box to create a "trough anomaly" (Figure 6a). The trough anomaly thus indicates how different the box SST_{adj} is from that of the IC. By doing this, we remove any interannual variability in magnitude that results from changes in the IC temperature itself as opposed to more or less AW intruding onto the shelf. A less negative anomaly means that trough waters are almost as warm as those offshore (IC region) while a more negative anomaly means that the trough is considerably colder than the IC. Any box covered in sea ice is assumed to be at the freezing temperature of seawater (−1.8°C). To determine thresholds for quantifying when AW temperatures are present at the surface within the trough, we compare anomalies found for all of the pixels within the IC and EGCC boxes, which represent AW and PW end members, respectively. More than 99% of IC pixels have anomalies above −1.5°C, while anomalies within the EGCC tend to be more negative (Figure S8). Using this

distinction, we consider a box to have AW at the surface when monthly trough anomalies are greater than −1.5°C (Figure 6b). We determine an annual mean for the location of the −1.5°C contour along the transect after removing the months where cloud cover obscures part of the transect and makes identification of the −1.5°C contour uncertain. Our results are not sensitive to slight variations in threshold choices.

Instances of small amplitude anomalies in the trough temperatures are associated with AW inflow onto the shelf (Sutherland et al., 2013) and we find that AW spread furthest inshore in 2003 and 2014–2018, while it was most consistently offshore in 2006–2008 and 2011–2012 (Figure 6b). In 2003 and 2018, AW extended along the entire trough (inshore of box 3) nearly year-round. Conversely, PW extended up to the continental shelf break for more than half of the year in 2007 and 2008 with little to no AW on the shelf during that time. The cross-shelf extent of AW intrusion has a strong negative correlation with the ShTr SST_{adj} ($r = -0.76$, $p < 0.001$; i.e., warm water farther inshore corresponds to a warmer SST_{adj}), although AW intrudes furthest inshore after 2014, which does not coincide with similarly extreme ShTr temperatures. The earlier periods of farthest intrusion, 2003 and 2010, are consistent with times of anomalously warm IC, however, the later period is not (Figure 4). Explicitly, this means that the temperature variability of the upper Irminger Sea region (IC box) is not always indicative of the extent of AW intrusions onto the shelf. Even as the Irminger Sea has been cooling, since 2010, the AW is intruding deeper onto the shelf and – presumably – influencing the waters flowing into Sermilik Fjord at depth.

4. Discussion

4.1. Reliable Application of Sea Surface Temperatures

While the MODIS record provides a high-temporal, long-duration time series of SSTs, significant challenges have slowed widespread application of this data set to quantify ocean water properties in the vicinity of glaciers. Frequent cloud and sea ice cover lead to few measurements of the ocean surface despite the, on average, 15 scans acquired per day, and weaknesses in the built-in SST masking protocols mean that the boxed SST products can often have cloud or ice contamination and tendency toward cold biases around Greenland (Jia & Minnett, 2020; Szczodrak et al., 2014). Regionally, SSTs are influenced by the relatively fresh PW and meltwater found near the coast and in some locations provide little information on the deeper AW temperatures on the continental shelf (Sutherland et al., 2013). Our work, however, shows that with adjustments for diurnal and seasonal variability, SSTs in certain regions can provide a reliable measure of upper ocean temperatures, and in the case of Sermilik Fjord, provide a measure of the AW temperatures entering a glacial fjord at depth.

In order to use MODIS skin SSTs in the polar regions as a measure of upper ocean temperatures, additional processing and consideration needs to be given to the Level 3 V2014 SST products provided by the NASA Ocean Biology Processing Group (Jia & Minnett, 2020). Sea ice must be directly masked (Figure S2a), seasonal skewing of the daytime and nighttime products in polar regions must be accounted for (Figure S1b), and diurnal biases between day- and nighttime products corrected (Figure S4; Kilpatrick et al., 2015; Minnett, 2003). We find that differences between the daytime and nighttime products can be large here (as much as 0.9°C between monthly averages) and daytime products skew observations toward the summer season when air temperature changes more strongly influence the SST signal. We also show that *SST* variability driven by air-sea interactions in non-winter months can be removed to obtain an SST_{adj} that is more closely linked with upper ocean temperature (Figure 3). This daytime/summertime bias is important because most previous research using MODIS SSTs around Greenland use daytime products (Howat et al., 2008, 2010; Sutherland et al., 2013), and any research using summertime SSTs (e.g., Andresen et al., 2012; Murray et al., 2010) may be measuring an SST signal strongly tied to atmospheric temperature, rather than the upper ocean.

For the ShTr region, the resultant SST_{adj} is also found to be representative ($r^2 = 0.53$) of temperatures observed at 290 m at a mooring near the mouth of Sermilik Fjord, year-round. We attribute this link to the fact that the AW flowing into the trough is the same water that enters the fjord at depth, 80 km downstream, beneath the EGCC, consistent with earlier studies. Absolute *SST* observations (Figure 5c) are consistent with the findings of Sutherland et al. (2013) who find that "uncorrected" summertime SST in the ShTr region do not significantly correlate with deeper trough water temperatures – below 200 m where AW is primarily

found – making uncorrected SST unreliable for monitoring them. Once the higher frequency imprinted atmospheric variability in non-winter months has been removed, as we have done in this study, however, the relationship between these SST_{adj} values and subsurface water temperatures becomes significant, albeit with more uncertainty than the respective wintertime relationship (winter RMSE = 0.57°C, non-winter RMSE = 0.70°C; Figures 3 and 5). For this reason, non-wintertime ShTr SST_{adj} can serve as a useful proxy for tracking subsurface water temperatures flowing into the fjord as long as the higher uncertainty associated with them does not exceed the variability in the ocean temperature signal. This may make the non-wintertime subsurface AW estimates inadequate for locations that experience less than a few degrees of water temperature variability.

While ShTr SST_{adj} serves as an estimate for the AW temperatures flowing into the fjord, the connection to deeper waters varies across the region based on differences in stratification, mixing patterns, and water masses present, therefore it is unclear to what extent SST_{adj} can serve as a proxy for subsurface waters in other locations. Many studies have shown large horizontal changes in the properties of the water column between the coast and offshore of the continental break near Sermilik Fjord (e.g., Harden et al., 2014; Rudels et al., 2002; Sutherland & Pickart, 2008). The upper water column within the IC is made up entirely of AW and we show that the SST_{adj} has a significant correlation ($r = 0.32$, $p = 0.02$) with the offshore OOI mooring temperature record from 180 m. The depth over which this correlation holds, presumably, varies seasonally and interannual with the depth of the mixed layer (near-surface to >1,500 m; de Jong et al., 2018). With a strong pycnocline between PW and AW serving as a barrier between the surface and subsurface waters along the coast (Harden et al., 2014; Straneo et al., 2010), SST_{adj} over the EGCC are indicative of surface PW, and have a much weaker or insignificant connection to the AW flowing below. This holds for the EGCC except when intrusions of water from the IC mix horizontally into it, which is not uncommon (Sutherland & Pickart, 2008). Seasonal changes in the stratification and mixing that stem from changes in freshwater input (e.g., sea ice or glacial runoff and melt; Stroh et al., 2015), wind speeds, and solar heating (Donlon et al., 2002; Minnett, 2003) will also impact the correlation between SST_{adj} and subsurface waters. Therefore, the choice of SST sampling location heavily impacts what information can be ascertained and the oceanography of each location must be well understood to use SSTs reliably.

Averaging windows used in the analyses also impact the relationships that can be found between SST, atmosphere, and water temperatures, and caveats exist for those we have chosen herein. In the sensitivity test for air temperature/SST linear relationships, we found that daily temperatures provided the most consistent and physically explainable seasonal A_m values for all three regions (Figure S6). While using daily temperatures for this correction accounts for diurnal solar heating and turbulence processes that occur on the order of a few hours, they do not capture processes that occur on timescales of a few days, such as inertial mixed layer currents (Donlon et al., 2002; Garwood, 1979). Therefore, some SST_{adj} variability may still be attributable to the atmosphere. Conversely, any sub-daily diurnal air-temperature/SST_{adj} co-variability (ascertained from single-scan MODIS Level 2 SSTs) may provide valuable information about diurnal relationships, but this variability is averaged out in the making of the Level 3 SST product. In examining the SST/subsurface mooring temperature relationship, we found that monthly averages provided the strongest and most robust linear relationships (Figure 5), which makes sense based on the previously measured shelf water velocities (Sutherland & Pickart, 2008) and the expected 1 to >10 days lag time between waters reaching the ShTr box and fjord mouth mooring 80 km inshore. These velocities and therefore, ocean temperatures likely fluctuate substantially with wind forcing and current transport (Le Bras et al., 2018; Sutherland & Pickart, 2008). Averaging to monthly windows means that upper ocean variability on shorter timescales, which may play an important role in glacier-ocean interactions, will go undetected. While outside the scope of this work, studies that incorporate mooring water velocities or co-located SST/mooring locations could better quantify sub-monthly upper ocean variability.

4.2. Historical Subsurface Water Temperatures and Implications

Our results provide two key insights into the Sermilik Fjord/shelf system. First, AW temperatures offshore within the IC are not necessarily indicative of coastal AW temperatures, which feed Sermilik Fjord. Instead, by the time it reaches the ShTr region, AW is much colder than the IC box, indicating dilution as it crosses the continental shelf (Figure 4). Second, we find that warmer waters intruded further inshore in the early

2000s until early 2005 (consistent with the sediment-based reconstruction of Andresen et al., 2012), which generally corresponds to changes in ice discharge patterns at Helheim Glacier (Figure 6; King et al., 2020). These combined observations indicate that the variability in AW temperatures found at depth nearshore result from an interplay of AW intruding onto the shelf and EGCC water, and that the relative fraction of these vary in time. These findings also highlight that satellite-derived SSTs can provide previously unobserved context for spatially or temporally limited field measurements.

Variability observed in the ShTr cannot be explained by IC and EGCC variability taken separately – which represent the AW and PW end members – but is a time-varying combination of the two (Figure 4). Notably, we find that the ShTr SST_{adj} did not always correlate with warmer AW in the IC from which the trough water is derived. The ShTr SST_{adj} instead warms when our analyses show that waters with properties similar to the IC intrude further onto the shelf (Figure 6). This linkage is most notable in the years when the ShTr SST_{adj} cooled while IC temperatures remained warm from 2005 to 2009 and after 2012 (Figure 6b). We infer that the varying dilution of AW as it crosses the continental shelf controls the ShTr SST_{adj}. These findings suggest that while there is a direct connection between the North Atlantic Ocean and Sermilik Fjord (Andresen et al., 2012; Straneo et al., 2010), the cooling of AW as it crosses the continental shelf varies interannually, making offshore IC temperatures a poor indicator for the waters entering the fjord.

Within the 19-year record, months with the smallest differences between the ShTr and IC SST_{adj} (Figure 4) are indicative of reduced AW dilution as it crosses the continental shelf (Moore et al., 2014; Straneo et al., 2010). If we take ShTr temperatures to be representative of the AW temperature entering the fjord, this suggests that the waters flowing into the fjord at depth were similar to those in the IC in the early 2000s, briefly in late 2009 to 2010, and in 2014–2018. These were also the years that exhibited the least change in ShTr SST_{adj} across the shelf and, thus, when AW intruded furthest onto the continental shelf (Figure 6b). We hypothesize that years with a more extended AW intrusion and warmer trough temperatures may also correspond with higher AW volume transport, but that analysis is outside of the purview of this study. The mechanisms driving AW dilution variability may be associated with tidal cycles, passing cyclonic eddies (Bruce, 1995; Sutherland & Pickart, 2008; Sutherland et al., 2013), current transport variability (Murray et al., 2010), wind patterns (Le Bras et al., 2018), or another phenomena.

The ShTr SST_{adj} record indicates that fluctuations in subsurface AW temperature and intrusion coincide with some of the variability in discharge rates previously found at Helheim Glacier for the same time period, but this relationship is not straightforward (Figures 6b and 6c). AW spreads inshore more consistently and the ShTr SST_{adj} was increasing to their warmest values during the early 2000s when Helheim Glacier experienced ice front retreat (Howat et al., 2005), thinning (Stearns & Hamilton, 2007), and heightened discharge rates (Howat et al., 2007; King et al., 2018). The glacier also decelerated and re-advanced from 2006 to 2008 (Howat et al., 2007; Schild & Hamilton, 2013) when the ShTr SST_{adj} was the coldest on record, though notably offshore AW temperatures had not measurably changed. This cooling likely resulted from weaker AW intrusion onto the continental shelf (Figure 6) and therefore, greater AW dilution as it flowed toward Helheim. In 2010, on the other hand, the ShTr SST_{adj} was relatively warm (>3.5°C annual average) and AW further intruded, although Helheim did not experience substantial increases in ice discharge (King et al., 2018, 2020), which may have been driven by a host of other environmental factors influencing glacier discharge rates (e.g., air temperature, glacier configuration, mélange rigidity; e.g., Carr et al., 2013; Joughin et al., 2012). While more work must be done to investigate mechanisms and the nature of these linkages, our work supports the notion that warmer waters flowing into the fjord from the shelf trough may have played a role in the glacier variability, especially in the early 2000s (e.g., Howat et al., 2008; Millan et al., 2018).

5. Conclusions

We produce upper ocean temperature records for three regions on the continental shelf near Sermilik Fjord using a composite of the MODIS Level 3 daytime and nighttime SST V2014.0 products (Figure 2). We find that *SST* in the study regions has a monthly varying linear relationship with air temperature that, once removed, produces a record indicative of the upper ocean. The SST_{adj} values from the ShTr region then have a strong linear relationship with subsurface water temperatures from a mooring located near Sermilik Fjord mouth at 290 m (Harden et al., 2014; Jackson et al., 2014), albeit with higher uncertainty in the summer

months (winter RMSE = 0.57°C and summer RMSE = 0.67°C). This relationship confirms that AW in the ShTr region is linked with subsurface water - which ultimately continues inshore beneath the EGCC to the mooring location where it feeds the fjord. Our records indicate that upper ocean temperatures in all three regions, and at depth in the case of the ShTr, were warmest in the early 2000s when Helheim experienced rapid retreat, supporting previous ideas that ocean warming played a role in the retreat.

Comparison of the upper ocean temperature variability in the three regions show that, while there is a direct connection between the North Atlantic Ocean and the bathymetric trough leading to Sermilik Fjord (Straneo et al., 2010), the dilution of AW as it flows across the shelf from the IC varies substantially over long timescales. This variability may be indicative of driving mechanisms that are linked to large-scale multi-year climate oscillations. The extent to which AW intrudes onto the shelf correlates strongly with inferred subsurface AW temperatures on the inner shelf, indicating that this intrusion plays a key role in setting the properties of the heat-carrying waters that flow into Sermilik Fjord at depth. Inferences cannot be directly made between North Atlantic warming and AW changes on the continental shelf near Sermilik Fjord. These findings have important implications for models that seek to resolve ocean temperatures and transport paths within the region.

With proper consideration of the physical processes affecting the measurements, SSTs show promise in applications to a wide range of polar oceanography and glaciology questions. The applicability of SSTs has vast spatial and temporal variability, varies with the SST product used (i.e., daytime or nighttime), and depends heavily on the specific oceanography of the location being explored. The identification of the relevant water masses and locations will need to be informed on a case-to-case basis. However, we believe that this method can be generalized to other systems in Greenland, especially in southeast Greenland where other deeply grounded outlet glaciers may share similar AW sources and regional forcings (Harden et al., 2014; Jackson et al., 2014; Millan et al., 2018; Straneo et al., 2010; Sutherland et al., 2014), including three of the largest contributors of ice discharge in Greenland: Helheim Glacier, Kangerdlugssuaq Glacier, and Køge Bugt (Enderlin et al., 2014; King et al., 2018; Rignot & Kanagaratnam, 2006). The new SST method described herein provides expanded ocean observations that complement sparse field records and may help to give a better mechanistic understanding of the ocean's role in Greenland glacier dynamics. Further work will continue to expand contextual understanding around the Greenland Ice Sheet both where long-standing field measurements have been acquired and where none exist.

Data Availability Statement

Processed data used in this manuscript are permanently archived at the Arctic Data Center (https://doi.org/10.18739/A2348GH20). The Python Jupyter Notebook processing and analysis code is available at https://doi.org/10.5281/zenodo.4305125. Users of the code should contact the author to ensure reasonable applications of the method. The Sermilik Fjord mouth mooring data used in this study are available at the National Oceanographic Data Center (https://data.nodc.noaa.gov/cgi-bin/iso?id=gov.noaa.nodc:0127325 and 0127320). The OOI mooring data were produced by FS from the Ocean Observatories Initiative. Level 3 MODIS SST data can be found at search.earthdata.nasa.gov, and ECMWF ERA-5 data ares located at www.ecmwf.int.

Acknowledgments
The authors gratefully acknowledge the National Aeronautics and Space Administration (NASA), the U.S. National Science Foundation (NSF), and the Cooperative Institute for Research in Environmental Sciences (CIRES). This work was supported by NASA Headquarters under a NASA Earth and Space Science Fellowship Program – Grant (NNX16AO33H). This material is also based upon work supported by the NSF Graduate Research Fellowship Program under grant DGE1650115. Any opinions, findings, and conclusions or recommendations expressed in this material are those of the authors and do not necessarily reflect the views of the NSF. F. Straneo and J. Holte were supported through NSF OCE-1657601 and the Heising-Simons Foundation. Thanks also go to the two reviewers for their comments that greatly improved the quality of this study.

References

Ackerman, S. A., Strabala, K. I., Menzel, W. P., Frey, R. A., Moeller, C. C., & Gumley, L. E. (1998). Discriminating clear sky from clouds with MODIS. *Journal of Geophysical Research*, *103*(D24), 32141–32157. https://doi.org/10.1029/1998jd200032

Andresen, C. S., Straneo, F., Ribergaard, M. H., Bjørk, A. A., Andersen, T. J., Kuijpers, A., et al. (2012). Rapid response of Helheim Glacier in Greenland to climate variability over the past century. *Nature Geoscience*, *5*(1), 37–41. https://doi.org/10.1038/ngeo1349

Bacon, S., Marshall, A., Holliday, N. P., Aksenov, Y., & Dye, S. R. (2014). Seasonal variability of the East Greenland Coastal Current. *Journal of Geophysical Research: Oceans*, *119*(6), 3967–3987. https://doi.org/10.1002/2013jc009279

Bacon, S., Reverdin, G., Rigor, I. G., & Snaith, H. M. (2002). A freshwater jet on the east Greenland shelf. *Journal of Geophysical Research*, *107*(C7), 51–516. https://doi.org/10.1029/2001jc000935

Beaird, N. L., Straneo, F., & Jenkins, W. (2018). Export of strongly diluted Greenland meltwater from a major glacial fjord. *Geophysical Research Letters*, *45*(9), 4163–4170. https://doi.org/10.1029/2018gl077000

Bevan, S. L., Luckman, A. J., Benn, D. I., Cowton, T., & Todd, J. (2019). Warming of SE Greenland shelf waters in 2016 primes large glacier for runaway retreat. *The Cryosphere Discussions*, 1–16. https://doi.org/10.5194/tc-2018-260

Bruce, J. G. (1995). Eddies southwest of the Denmark Strait. *Deep Sea Research Part I: Oceanographic Research Papers*, *42*(1), 13–29. https://doi.org/10.1016/0967-0637(94)00040-y

Carr, J. R., Stokes, C. R., & Vieli, A. (2013). Recent progress in understanding marine-terminating Arctic outlet glacier response to climatic and oceanic forcing. *Progress in Physical Geography: Earth and Environment*, *37*(4), 436–467. https://doi.org/10.1177/0309133313483163

Chang, P. (1993). Seasonal cycle of sea surface temperature and mixed layer heat budget in the tropical Pacific Ocean. *Geophysical Research Letters*, *20*(19), 2079–2082. https://doi.org/10.1029/93gl02374

Christoffersen, P., Mugford, R. I., Heywood, K. J., Joughin, I., Dowdeswell, J. A., Syvitski, J. P. M., et al. (2011). Warming of waters in an East Greenland fjord prior to glacier retreat: Mechanisms and connection to large-scale atmospheric conditions. *The Cryosphere*, *5*(3), 701–714. https://doi.org/10.5194/tc-5-701-2011

Copernicus Climate Change Service. (2017). *ERA5: Fifth generation of ECMWF atmospheric reanalyzes of the global climate*. https://cds.climate.copernicus.eu/cdsapp#!/home

de Jong, M. F., Oltmanns, M., Karstensen, J., & de Steur, L. (2018). Deep convection in the Irminger Sea observed with a dense mooring array. *Oceanog*, *31*(1), 50–59. https://doi.org/10.5670/oceanog.2018.109

de Jong, M. F., & Steur, L. d. (2016). Strong winter cooling over the Irminger Sea in winter 2014-2015, exceptional deep convection, and the emergence of anomalously low SST. *Geophysical Research Letters*, *43*(13), 7106–7113. https://doi.org/10.1002/2016gl069596

Denman, K. L. (1973). A time-dependent model of the upper ocean. *Journal of Physical Oceanography*, *3*(2), 173–184. https://doi.org/10.1175/1520-0485(1973)003<0173:atdmot>2.0.co;2

Donlon, C., Minnett, P., & Gentemann, C. (2002). Toward improved validation of satellite sea surface skin temperature measurements for climate research. *Journal of Climate*, *15*(4), 353–369.

Eastwood, S., Le Borgne, P., Péré, S., & Poulter, D. (2011). Diurnal variability in sea surface temperature in the Arctic. *Remote Sensing of Environment*, *115*(10), 2594–2602. https://doi.org/10.1016/j.rse.2011.05.015

Enderlin, E. M., Howat, I. M., Jeong, S., Noh, M.-J., van Angelen, J. H., & van den Broeke, M. R. (2014). An improved mass budget for the Greenland ice sheet. *Geophysical Research Letters*, *41*(3), 866–872. https://doi.org/10.1002/2013GL059010

Fettweis, X., Box, J. E., Agosta, C., Amory, C., Kittel, C., Lang, C., et al. (2017). Reconstructions of the 1900-2015 Greenland ice sheet surface mass balance using the regional climate MAR model. *The Cryosphere*, *11*(2), 1015–1033. https://doi.org/10.5194/tc-11-1015-2017

Frankignoul, C., & Hasselmann, K. (1977). Stochastic climate models, Part II Application to sea-surface temperature anomalies and thermocline variability. *Tellus*, *29*(4), 289–305. https://doi.org/10.1111/j.2153-3490.1977.tb00740.x10.3402/tellusa.v29i4.11362

Garwood, R. W. (1979). Air-sea interaction and dynamics of the surface mixed layer. *Reviews of Geophysics and Space Physics*, *7*(17).

Gautier, C., Peterson, P., & Jones, C. (1998). Ocean surface air temperature derived from multiple data sets and artificial neural networks. *Geophysical Research Letters*, *25*(22), 4217–4220. https://doi.org/10.1029/1998gl900086

Harden, B. E., Straneo, F., & Sutherland, D. A. (2014). Moored observations of synoptic and seasonal variability in the East Greenland Coastal Current. *Journal of Geophysical Research: Oceans*, *119*(12), 8838–8857. https://doi.org/10.1002/2014JC010134

Hersbach, H., Bell, B., Berrisford, P., Hirahara, S., Horányi, A., Muñoz-Sabater, J., et al. (2020). The ERA5 global reanalysis. *Quarterly Journal of the Royal Meteorological Society*, *146*, 1999–2049. https://doi.org/10.1002/qj.3803

Holland, D. M., Thomas, R. H., de Young, B., Ribergaard, M. H., & Lyberth, B. (2008). Acceleration of Jakobshavn Isbræ triggered by warm subsurface ocean waters. *Nature Geoscience*, *1*, 659–664. https://doi.org/10.1038/ngeo316

Howat, I. M., Box, J., Ahn, Y., & Herrington, A. (2010). Seasonal variability in the dynamics of marine-terminating outlet glaciers in Greenland. *Journal of Glaciology*, *56*(198), 601–613. https://doi.org/10.3189/002214310793146232

Howat, I. M., Joughin, I., Fahnestock, M., Smith, B., & Scambos, T. (2008). Synchronous retreat and acceleration of southeast Greenland outlet glaciers 2000-06: Ice dynamics and coupling to climate. *Journal of Glaciology*, *54*(187). https://doi.org/10.3189/002214308786570908

Howat, I. M., Joughin, I., & Scambos, T. A. (2007). Rapid changes in ice discharge from Greenland Outlet Glaciers. *Science*, *315*(5818), 1559–1561. https://doi.org/10.1126/science.1138478

Howat, I. M., Joughin, I., Tulaczyk, S., & Gogineni, S. (2005). Rapid retreat and acceleration of Helheim Glacier, east Greenland. *Geophysical Research Letters*, *32*(22). https://doi.org/10.1029/2005GL024737

IMBIE Team. (2019). Mass balance of the Greenland Ice Sheet from 1992 to 2018. *Nature*. https://doi.org/10.1038/s41586-019-1855-2

Inall, M. E., Murray, T., Cottier, F. R., Scharrer, K., Boyd, T. J., Heywood, K. J., & Bevan, S. L. (2014). Oceanic heat delivery via Kangerdlugssuaq Fjord to the south-east Greenland ice sheet. *Journal of Geophysical Research: Oceans*, *119*(2), 631–645. https://doi.org/10.1002/2013jc009295

Jackson, R. H., & Straneo, F. (2016). Heat, salt, and freshwater budgets for a glacial fjord in Greenland. *Journal of Physical Oceanography*, *46*(9), 2735–2768. https://doi.org/10.1175/JPO-D-15-0134.1

Jackson, R. H., Straneo, F., & Sutherland, D. A. (2014). Externally forced fluctuations in ocean temperature at Greenland glaciers in non-summer months. *Nature Geoscience*, *7*(7), 503–508. https://doi.org/10.1038/ngeo2186

Jaswal, A. K., Singh, V., & Bhambak, S. R. (2012). Relationship between sea surface temperature and surface air temperature over Arabian Sea, Bay of Bengal and Indian Ocean. *The Journal of Indian Geophysical Union*, *16*, 41–53.

Jia, C., & Minnett, P. J. (2020). High latitude sea surface temperatures derived from MODIS infrared measurements. *Remote Sensing of Environment*, *251*, 112094. https://doi.org/10.1016/j.rse.2020.112094

Johannessen, O. M., Korablev, A., Miles, V., Miles, M. W., & Solberg, K. E. (2011). Interaction between the warm subsurface Atlantic Water in the Sermilik Fjord and Helheim Glacier in southeast Greenland. *Surveys in Geophysics*, *32*(4–5), 387–396. https://doi.org/10.1007/s10712-011-9130-6

Jones, C., Peterson, P., & Gautier, C. (1999). A new method for deriving ocean surface specific humidity and air temperature: An artificial neural network approach. *Journal of Applied Meteorology*, *38*(8), 1229–1245. https://doi.org/10.1175/1520-0450(1999)038<1229:anmfdo>2.0.co;2

Joughin, I., Alley, R. B., & Holland, D. M. (2012). Ice-Sheet response to oceanic forcing. *Science*, *338*(6111), 1172–1176. https://doi.org/10.1126/science.1226481

Kawai, Y., & Wada, A. (2007). Diurnal sea surface temperature variation and its impact on the atmosphere and ocean: A review. *Journal of Oceanography*, *63*(5), 721–744. https://doi.org/10.1007/s10872-007-0063-0

Khan, S. A., Kjær, K. H., Bevis, M., Bamber, J. L., Wahr, J., Kjeldsen, K. K., et al. (2014). Sustained mass loss of the northeast Greenland ice sheet triggered by regional warming. *Nature Climate Change*, *4*(4), 292–299. https://doi.org/10.1038/nclimate2161

Kilpatrick, K. A., Podestá, G., Walsh, S., Williams, E., Halliwell, V., Szczodrak, M., et al. (2015). A decade of sea surface temperature from MODIS. *Remote Sensing of Environment*, *165*, 27–41. https://doi.org/10.1016/j.rse.2015.04.023

Kilpatrick, K. A., Podestá, G., Williams, E., Walsh, S., & Minnett, P. J. (2019). Alternating decision trees for cloud masking in MODIS and VIIRS NASA sea surface temperature products. *Journal of Atmospheric and Oceanic Technology*, *36*, 387. https://doi.org/10.1175/JTECH-D-18-0103.1

King, M. D., Howat, I. M., Candela, S. G., Noh, M. J., Jeong, S., Noël, B. P. Y., et al. (2020). Dynamic ice loss from the Greenland Ice Sheet driven by sustained glacier retreat. *Communications Earth Environment*, *1*(1), 1. https://doi.org/10.1038/s43247-020-0001-2

King, M. D., Howat, I. M., Jeong, S., Noh, M. J., Wouters, B., Noël, B., & van den Broeke, M. R. (2018). Seasonal to decadal variability in ice discharge from the Greenland Ice Sheet. *The Cryosphere*, *12*(12), 3813–3825. https://doi.org/10.5194/tc-12-3813-2018

Koizumi, M. (1956). Researches on the Variations of oceanographic conditions in the region of the ocean weather station "Extra" in the North Pacific Ocean (VI). *Papers in Meteorology and Geophysics*, *7*(3), 322–326. https://doi.org/10.2467/mripapers1950.7.3_32210.2467/mripapers1950.7.3_322

Konda, M., Imasato, N., & Shibata, A. (1996). A new method to determine near-sea surface air temperature by using satellite data. *Journal of Geophysical Research*, *101*(C6), 14349–14360. https://doi.org/10.1029/96jc00796

Kraus, E. B., & Turner, J. S. (1967). A one-dimensional model of the seasonal thermocline II. The general theory and its consequences. *Tellus*, *19*(1), 98–106. https://doi.org/10.1111/j.2153-3490.1967.tb01462.x10.3402/tellusa.v19i1.9753

Krauss, W. (1995). Currents and mixing in the Irminger Sea and in the Iceland Basin. *Journal of Geophysical Research*, *100*(C6), 10851–10871. https://doi.org/10.1029/95jc00423

Le Bras, I., Straneo, F., Holte, J., & Holliday, N. P. (2018). Seasonality of freshwater in the east Greenland current system from 2014 to 2016. *Journal of Geophysical Research: Oceans*, *123*, 8828–8848. https://doi.org/10.1029/2018JC014511

Luckman, A., Murray, T., de Lange, R., & Hanna, E. (2006). Rapid and synchronous ice-dynamic changes in East Greenland. *Geophysical Research Letters*, *33*(3). https://doi.org/10.1029/2005GL025428

Mankoff, K. D., Solgaard, A., Colgan, W., Ahlstrøm, A. P., Khan, S. A., & Fausto, R. S. (2020). Greenland Ice Sheet solid ice discharge from 1986 through March 2020. *Earth System Science Data*, *12*(2), 1367–1383. https://doi.org/10.5194/essd-12-1367-2020

Millan, R., Rignot, E., Mouginot, J., Wood, M., Bjørk, A. A., & Morlighem, M. (2018). Vulnerability of southeast Greenland Glaciers to Warm Atlantic Water from operation IceBridge and ocean melting Greenland data. *Geophysical Research Letters*, *45*(6), 2688–2696. https://doi.org/10.1002/2017GL076561

Minnett, P. J. (2003). Radiometric measurements of the sea-surface skin temperature: The competing roles of the diurnal thermocline and the cool skin. *International Journal of Remote Sensing*, *24*(24), 5033–5047. https://doi.org/10.1080/0143116031000095880

Moon, T., Joughin, I., Smith, B., & Howat, I. (2012). 21st-century evolution of Greenland Outlet Glacier velocities. *Science*, *336*(6081), 576–578. https://doi.org/10.1126/science.1219985

Moore, G. W. K., Straneo, F., & Oltmanns, M. (2014). Trend and interannual variability in southeast Greenland Sea Ice: Impacts on coastal Greenland climate variability. *Geophysical Research Letters*, *41*(23), 8619–8626. https://doi.org/10.1002/2014gl062107

Morlighem, M., Williams, C. N., Rignot, E., An, L., Arndt, J. E., Bamber, J. L., et al. (2017). BedMachine v3: Complete bed topography and ocean bathymetry mapping of Greenland from multibeam echo sounding combined with mass conservation. *Geophysical Research Letters*, *44*(21), 11051–11061. https://doi.org/10.1002/2017gl074954

Mouginot, J., Rignot, E., Bjørk, A. A., van den Broeke, M., Millan, R., Morlighem, M., et al. (2019). Forty-six years of Greenland Ice Sheet mass balance from 1972 to 2018. *Proceedings of the National Academy of Sciences of the United States of America*, *116*(19), 9239–9244. https://doi.org/10.1073/pnas.1904242116

Mouginot, J., Rignot, E., Scheuchl, B., Fenty, I., Khazendar, A., Morlighem, M., et al. (2015). Fast retreat of Zachariae Isstrom, northeast Greenland. *Science*, *350*(6266), 1357–1361. https://doi.org/10.1126/science.aac7111

Murray, T., Scharrer, K., James, T. D., Dye, S. R., Hanna, E., Booth, A. D., et al. (2010). Ocean regulation hypothesis for glacier dynamics in southeast Greenland and implications for ice sheet mass changes. *Journal of Geophysical Research*, *115*(F3). https://doi.org/10.1029/2009JF001522

Ocean Biology Processing Group, O. E. L., & NASA Goddard Space Flight Center. (2014a). *MODIS-Aqua Ocean Color Data*. https://earthdata.nasa.gov/http://dx.doi.org/10.5067/AQUA/MODIS_OC.2014.0

Ocean Biology Processing Group, O. E. L., & NASA Goddard Space Flight Center. (2014b). *MODIS-Terra Ocean Color Data*. http://doi.org/10.5067/TERRA/MODIS_OC.2014.0

Price, J. F., Weller, R. A., & Pinkel, R. (1986). Diurnal cycling: Observations and models of the upper ocean response to diurnal heating, cooling, and wind mixing. *Journal of Geophysical Research*, *91*(C7), 8411–8427. https://doi.org/10.1029/jc091ic07p08411

Rignot, E., & Kanagaratnam, P. (2006). Changes in the velocity structure of the Greenland Ice Sheet. *Science*, *311*. https://doi.org/10.1126/science.1121381

Rudels, B., Fahrbach, E., Meincke, J., Budéus, G., & Eriksson, P. (2002). The East Greenland Current and its contribution to the Denmark Strait overflow. *ICES Journal of Marine Science*, *59*(6), 1133–1154. https://doi.org/10.1006/jmsc.2002.1284

Schild, K. M., & Hamilton, G. S. (2013). Seasonal variations of outlet glacier terminus position in Greenland. *Journal of Glaciology*, *59*(216), 759–770. https://doi.org/10.3189/2013jog12j238

Schulz, J., Meywerk, J., Ewald, S., & Schlüssel, P. (1997). Evaluation of satellite-derived latent heat fluxes. *Journal of Climate*, *10*(11), 2782–2795. https://doi.org/10.1175/1520-0442(1997)010<2782:eosdlh>2.0.co;2

Seabold, S., & Perktold, J. (2010). *Statsmodels: Econometric and statistical modeling with Python* (pp. 92–96). https://doi.org/10.25080/majora-92bf1922-011

Singh, R., Joshi, P. C., & Kishtawal, C. M. (2006). A new method to determine near surface air temperature from satellite observations. *International Journal of Remote Sensing*, *27*(14), 2831–2846. https://doi.org/10.1080/01431160500195234

Singh, R., Kishtawal, C. M., & Joshi, P. C. (2005). Estimation of monthly mean air-sea temperature difference from satellite observations using genetic algorithm. *Geophysical Research Letters*, *32*(2). https://doi.org/10.1029/2004gl021531

Stearns, L. A., & Hamilton, G. S. (2007). Rapid volume loss from two East Greenland outlet glaciers quantified using repeat stereo satellite imagery. *Geophysical Research Letters*, *34*(5). https://doi.org/10.1029/2006gl028982

Straneo, F., Curry, R. G., Sutherland, D. A., Hamilton, G. S., Cenedese, C., Våge, K., & Stearns, L. A. (2011). Impact of fjord dynamics and glacial runoff on the circulation near Helheim Glacier. *Nature Geoscience*, *4*, 322–327. https://doi.org/10.1038/ngeo1109

Straneo, F., Hamilton, G., Stearns, L., & Sutherland, D. (2016). Connecting the Greenland Ice Sheet and the Ocean: A case study of Helheim Glacier and Sermilik Fjord. *Oceanography*, *29*(4), 34–45. https://doi.org/10.5670/oceanog.2016.97

Straneo, F., Hamilton, G. S., Sutherland, D. A., Stearns, L. A., Davidson, F., Hammill, M. O., et al. (2010). Rapid circulation of warm subtropical waters in a major glacial fjord in East Greenland. *Nature Geoscience*, *3*(3), 182–186. https://doi.org/10.1038/ngeo764

Straneo, F., & Heimbach, P. (2013). North Atlantic warming and the retreat of Greenland's outlet glaciers. *Nature*, *504*(7478), 36–43. https://doi.org/10.1038/nature12854

Straneo, F., Sutherland, D. A., Holland, D., Gladish, C., Hamilton, G. S., Johnson, H. L., et al. (2012). Characteristics of ocean waters reaching Greenland's glaciers. *Annals of Glaciology*, *53*(60), 202–210. https://doi.org/10.3189/2012aog60a059

Stroh, J. N., Panteleev, G., Kirillov, S., Makhotin, M., & Shakhova, N. (2015). Sea-surface temperature and salinity product comparison against external in situ data in the Arctic Ocean. *Journal of Geophysical Research: Oceans*, *120*(11), 7223–7236. https://doi.org/10.1002/2015jc011005

Sutherland, D. A., & Pickart, R. S. (2008). The East Greenland Coastal Current: Structure, variability, and forcing. *Progress in Oceanography*, *78*(1), 58–77. https://doi.org/10.1016/j.pocean.2007.09.006

Sutherland, D. A., Straneo, F., & Pickart, R. S. (2014). Characteristics and dynamics of two major Greenland glacial fjords. *Journal of Geophysical Research: Oceans*, *119*(6), 3767–3791. https://doi.org/10.1002/2013JC009786

Sutherland, D. A., Straneo, F., Stenson, G. B., Davidson, F. J. M., Hammill, M. O., & Rosing-Asvid, A. (2013). Atlantic water variability on the SE Greenland continental shelf and its relationship to SST and bathymetry. *Journal of Geophysical Research: Oceans*, *118*(2), 847–855. https://doi.org/10.1029/2012JC008354

Sverdrup, H. U., Johnson, M. W., & Fleming, R. H. (1942). *The Oceans: Their Physics, Chemistry, and General Biology*. Prentice-Hall, Inc. Retrieved from http://ark.cdlib.org/ark:/13030/kt167nb66r/

Szczodrak, M., Minnett, P. J., & Evans, R. H. (2014). The effects of anomalous atmospheres on the accuracy of infrared sea-surface temperature retrievals: Dry air layer intrusions over the tropical ocean. *Remote Sensing of Environment*, *140*, 450–465. https://doi.org/10.1016/j.rse.2013.09.010

Våge, K., Pickart, R. S., Sarafanov, A., Knutsen, Ø., Mercier, H., Lherminier, P., et al. (2011). The Irminger Gyre: Circulation, convection, and interannual variability. *Deep Sea Research Part I: Oceanographic Research Papers*, *58*(5), 590–614. https://doi.org/10.1016/j.dsr.2011.03.001

van den Broeke, M., Bamber, J., Ettema, J., Rignot, E., Schrama, E., van de Berg, W. J., et al. (2009). Partitioning recent Greenland mass loss. *Science*, *326*(5955), 984–986. https://doi.org/10.1126/science.1178176

Virtanen, P., Gommers, R., Oliphant, T. E., Haberland, M., Reddy, T., Cournapeau, D., et al. (2020). SciPy 1.0: Fundamental algorithms for scientific computing in Python. *Nature Methods*, *17*(3), 261–272. https://doi.org/10.1038/s41592-019-0686-2

Walsh, K. M., Howat, I. M., Ahn, Y., & Enderlin, E. M. (2012). Changes in the marine-terminating glaciers of central east Greenland, 2000-2010. *The Cryosphere*, *6*(1), 211–220. https://doi.org/10.5194/tc-6-211-2012

References From the Supporting Information

Gentemann, C. L., Minnett, P. J., Le Borgne, P., & Merchant, C. J. (2008). Multi-satellite measurements of large diurnal warming events. *Geophysical Research Letters*, *35*(22). https://doi.org/10.1029/2008gl035730

Hastings, A. D. J. (1960). Environment of Southeast Greenland. https://doi.org/10.21236/ad0251797

Kilpatrick, K. A., Podestá, G. P., & Evans, R. (2001). Overview of the NOAA/NASA advanced very high resolution radiometer Pathfinder algorithm for sea surface temperature and associated matchup database. *Journal of Geophysical Research*, *106*(C5), 9179–9197. https://doi.org/10.1029/1999jc000065

Kumar, A., Minnett, P. J., Podestá, G., & Evans, R. H. (2003). Error characteristics of the atmospheric correction algorithms used in retrieval of sea surface temperatures from infrared satellite measurements: Global and regional aspects. *Journal of the Atmospheric Sciences*, *60*(3), 575–585. https://doi.org/10.1175/1520-0469(2003)060<0575:ecotac>2.0.co;2

McKinney, W. (2010). *Data structures for statistical computing in Python* (pp. 56–61). https://doi.org/10.25080/majora-92bf1922-00a

Minnett, P. J., Knuteson, R. O., Best, F. A., Osborne, B. J., Hanafin, J. A., & Brown, O. B. (2001). The marine-atmospheric emitted radiance interferometer: A high-accuracy, seagoing infrared spectroradiometer. *Journal of Atmospheric and Oceanic Technology*, *18*(6), 994–1013. https://doi.org/10.1175/1520-0426(2001)018<0994:tmaeri>2.0.co;2

Spreen, G., Kaleschke, L., & Heygster, G. (2008). Sea ice remote sensing using AMSR-E 89-GHz channels. *Journal of Geophysical Research*, *113*(C2). https://doi.org/10.1029/2005jc003384

Stramma, L., Cornillon, P., Weller, R. A., Price, J. F., & Briscoe, M. G. (1986). Large diurnal sea surface temperature variability: Satellite and in situ measurements. *Journal of Physical Oceanography*, *16*(5), 827–837. https://doi.org/10.1175/1520-0485(1986)016<0827:ldsstv>2.0.co;2

Sutherland, D. A., Pickart, R. S., Peter Jones, E., Azetsu-Scott, K., Jane Eert, A., & Ólafsson, J. (2009). Freshwater composition of the waters off southeast Greenland and their link to the Arctic Ocean. *Journal of Geophysical Research*, *114*(C5). https://doi.org/10.1029/2008JC004808